UC San Diego
UC San Diego Previously Published Works

Title

Tradeoffs of Source Coding, Channel Coding and Spreading in Frequency Selective Rayleigh Fading Channels

Permalink
https://escholarship.org/uc/item/1g40t1z3

Journal
The Journal of VLSI Signal Processing, 30(1/3)

ISSN
09225773

Authors
Zhao, Qinghua
Cosman, Pamela
Milstein, Laurence B

Publication Date
2002

DOI
10.1023/A:1014034506244

Peer reviewed

eScholarship.org Powered by the California Digital Library
University of California

Journal of VLSI Signal Processing 30, 7–20, 2002
© 2002 Kluwer Academic Publishers. Manufactured in The Netherlands.

Tradeoffs of Source Coding, Channel Coding and Spreading in Frequency Selective Rayleigh Fading Channels

QINGHUA ZHAO, PAMELA COSMAN AND LAURENCE B. MILSTEIN
Department of Electrical and Computer Engineering, University of California, San Diego. 9500 Gilman Drive, La Jolla, CA 92093-0407, USA

Received August 31, 2000; Revised June 26, 2001

Abstract. This paper investigates the tradeoffs of source coding, channel coding and spreading in CDMA systems. We consider a system consisting of an image source coder, a convolutional channel coder, an interleaver, and a direct sequence spreading module. With different allocations of bandwidth to source coding, channel coding and spreading, the system is analyzed over a frequency selective Rayleigh fading channel. The performance of the system is evaluated using the cumulative distribution function of peak signal-to-noise ratio. Tradeoffs of different components of the system are determined through simulations. We show that, for a given bandwidth, an optimal allocation of that bandwidth can be found. Tradeoffs among the parameters allow us to tune the system performance to specific requirements.

Keywords: bandwidth allocation, direct-sequence CDMA, frequency selective Rayleigh fading, image transmission over wireless channels, multiuser system, channel estimation

1. Introduction

Source coding, channel coding and spread spectrum are the three main components in a CDMA communication system. A number of studies have been performed on the joint design of source and channel coding algorithms to yield better system throughput (e.g., [1–3]). There also exists a body of research on the tradeoffs between channel coding and CDMA (e.g., [4–6]). In this work, we investigate the interrelationship among all three components.

Bandwidth is the major resource shared among the three components. Allocating more bandwidth to source coding allows more information from the source to be transmitted, but reduces the bandwidth available for both forward error correction (FEC) and spreading. For different compression methods and rates, the bit stream coming out of the source encoder is more or less sensitive to different types of error patterns. FEC and spreading protect the transmitted bits from noise and interference. Depending on the channel conditions and the characteristics of the source coded bit stream, the system performs better with either more FEC or more spreading.

Let r_s, r_c and M denote the source code rate (in bits per pixel, bpp), channel code rate, and processing gain, respectively. For a given bandwidth constraint and transmission time, our goal is to find the optimal set $(\hat{r}_s, \hat{r}_c, \hat{M})$ under the constraint

$$U \cdot r_s \cdot \frac{1}{r_c} \cdot M = C \Longrightarrow r_s \cdot \frac{1}{r_c} \cdot M = \frac{C}{U} = C_1, \quad (1)$$

where U is the number of pixels of the original image and C and C_1 are constants.

The paper is organized as follows. Section 2 introduces the source coding and channel coding. In Section 3, the bit error performance of the system is analyzed for a frequency selective Rayleigh fading channel; theoretical and simulation results are compared. Some representative results of tradeoffs among all three components are given in Section 4, and the conclusions are given in Section 5.

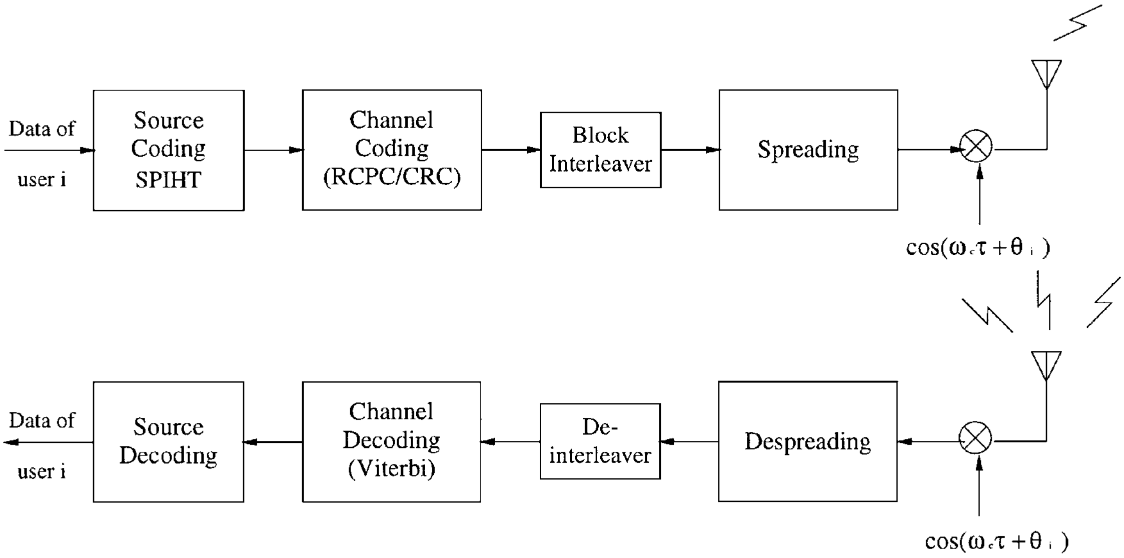

Figure 1. System overview.

2. Source Coding and Channel Coding

The system is shown in Fig. 1. In the following sections, we discuss each component in detail.

2.1. Source Coding

The source images are encoded using a lossy compression algorithm called Set Partitioning In Hierarchical Trees (SPIHT [7]). The encoded bit stream is progressive, i.e., bits which come first can be used to reconstruct a low quality version of the source image, and bits which come later can be decoded to produce successively higher quality versions. The SPIHT algorithm has excellent compression performance, however, it is very sensitive to errors. An error in one bit may lead to complete loss of synchronization in the source decoder, in which case attempting to decode the subsequent bits would cause the quality of the decoded image to deteriorate. Also, there is a small amount of image header information for the coded source bit stream (59 bits in most cases). This number is very small compared to the bit budget for almost all transmission rates of interest, so in all the analyses and simulations presented below, the header is assumed to be error-free.

2.2. Channel Coding

In Fig. 2 [8], source information bits are grouped into blocks of size N. A 16-bit CRC (Cyclic Redundancy

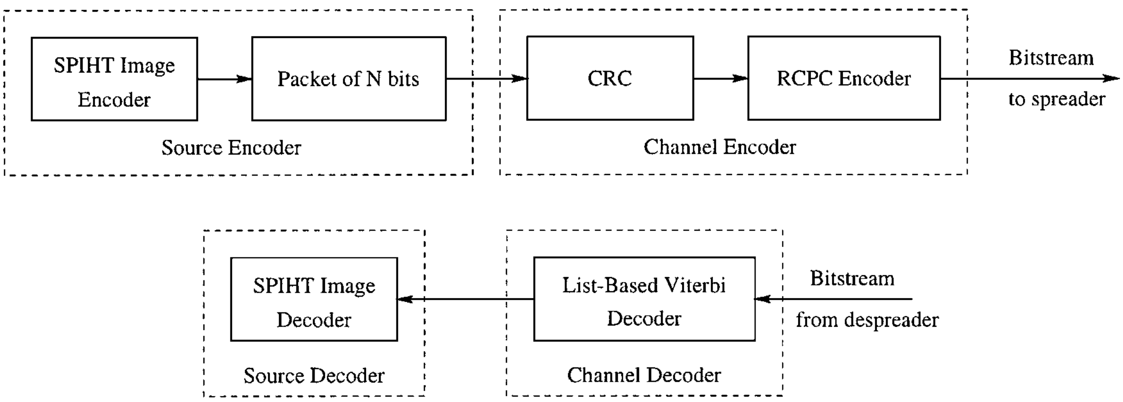

Figure 2. Source and channel coding block diagram.

Code) is added to each block. Then the block is convolutionally encoded using a Rate-Compatible Punctured Convolutional (RCPC) [9] code. At the receiver, the list-based Viterbi algorithm is used to find the best candidate in the trellis for the current block. Then the CRC detects whether there is an error. If there is an error, the second best candidate is found and the CRC is again checked, and so on. After checking the list of paths for a predetermined number of times, if the CRC check still declares an error, the source decoder discards this block and all subsequent blocks. The image is then reconstructed from the previously received blocks.

3. Direct Sequence CDMA

3.1. Signal and Channel Model

The coded data stream is spread, using direct sequence with a long spreading code, by a factor of M (the processing gain). Then the signal is transmitted using BPSK modulation. Assume there are K simultaneously active users in the system. The signature sequences of different users have a common chip rate of $1/T_c$, where $T_c = T/M$, and $1/T$ is the data bit rate (in bits per second). Let $a_k(t)$ denote the signature sequence waveform of the kth user, and let $a_j^{(k)}$ be the corresponding sequence elements, where $a_j^{(k)} \in (+1, -1)$. Then

$$a_k(t) = \sum_{j=-\infty}^{\infty} a_j^{(k)} P_{T_c}(t - jT_c), \tag{2}$$

where $P_{T_c}(t)$ is the chip pulse shape. For simplicity, a square-wave pulse is chosen, so that $P_{T_c} = 1$ for $0 \leq t < T_c$ and zero elsewhere. Similarly, the data signal may be written as

$$b_k(t) = \sum_{j=-\infty}^{\infty} b_j^{(k)} P_T(t - jT), \tag{3}$$

where $b_j^{(k)} \in (-1, 1)$. Therefore, the transmitted signal for the kth user is

$$s_k(t) = \mathrm{Re}\big[S_k(t)e^{j\omega_c t}\big], \tag{4}$$

where

$$S_k(t) = Aa_k(t)b_k(t)e^{j\theta_k}, \tag{5}$$

A is the magnitude of the transmitted signal, assumed to be the same for all users, ω_c is the common carrier frequency and θ_k is the phase of the kth user. Assuming asynchronous operation, the delay of user k relative to the reference user (user 0) is τ_k, $k = 1, \ldots, K-1$. The composite signal at the input to the channel is

$$s_T(t) = \mathrm{Re}\big[S_T(t)e^{j\omega_c t}\big], \tag{6}$$

where

$$S_T(t) = \sum_{k=0}^{K-1} Aa_k(t - \tau_k)b_k(t - \tau_k)e^{j\phi_k}, \tag{7}$$

$\phi_k = \theta_k - \omega_c\tau_k$, $\theta_0 = \tau_0 = 0$, $(\phi_k)_{k=1}^{K-1}$ are independent identically distributed (iid) random variables, uniformly distributed in $[0, 2\pi)$, and $(\tau_k)_{k=1}^{K-1}$ are iid random variables, uniformly distributed in $[0, T)$.

A tapped delay line is used to model the frequency selective Rayleigh fading channel. The signal at the output of the channel can be written as $r(t) = \mathrm{Re}\{R(t)e^{j\omega t}\}$, where

$$R(t) = \sum_{k=0}^{K-1}\sum_{l=0}^{L-1} \alpha_k^l(t)e^{j\theta_k^l(t)} S_k(t - lT_c - \tau_k) + n_W(t), \tag{8}$$

$n_W(t)$ is complex Gaussian noise with two sided power spectral density N_0, L is the number of resolvable multipaths, and $\alpha_k^l(t)e^{j\theta_k^l(t)}$ is a complex gain which represents the fading experienced by the kth user on the lth path, uncorrelated for different k and l, but correlated over time t (for convenience, we assume the fading is constant during each symbol duration). We assume all users are operating in a similar environment with a flat Multipath Intensity Profile (MIP), i.e., all α_k^l's are identically distributed with density function $p(\alpha) = \frac{\alpha}{\sigma^2} e^{\frac{-\alpha^2}{2\sigma^2}}$, and θ_i is uniformly distributed. For simplicity, we set

$$\mathrm{Var}\big[\alpha_k^l(t)\big] = 2\sigma^2 = 1.$$

3.2. RAKE Receiver and Trellis Structure

The RAKE receiver shown in Fig. 3 is used to resolve the L_R resolvable multipaths. Every T seconds at $T_{sa}^{(n)} = nT + (L_R - 1)T_c$, the RAKE output is sampled and fed into a soft decision decoder.

For the ith data bit of the reference user, the test statistic on the lth path of the RAKE is given by

$$g_{i,l} = AMb_i^{(0)}\alpha_0^l\big(T_{sa}^{(i)}\big)e^{j\theta_0^l(T_{sa}^{(i)})} + n_{Si,l} + n_{Mi,l} + n_{Wi,l}. \tag{9}$$

In (9), the first term on the right hand side is the signal component, and the last three terms correspond to self-interference, multi-access interference, and noise,

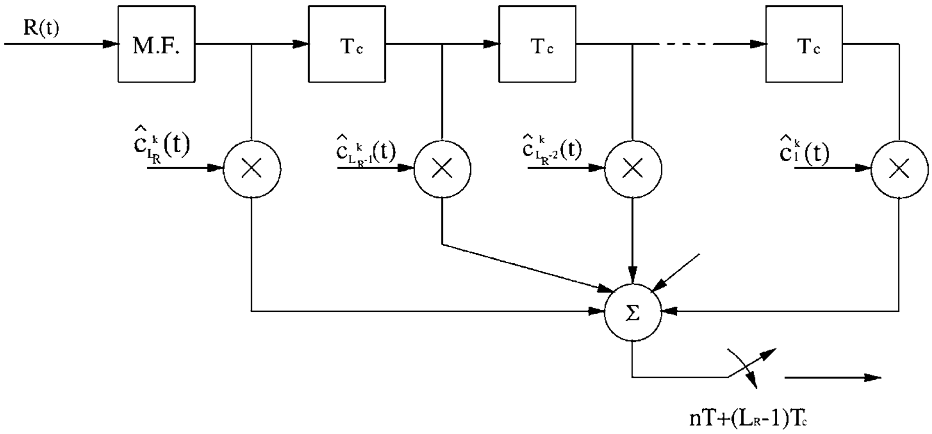

Figure 3. RAKE receiver model.

given by

$$n_{Si,l} = \sum_{s=0,s\neq 1}^{L-1} b_i^{(0)} \alpha_0^s\big(T_{sa}^{(i)}\big) e^{j\theta_0^s(T_{sa}^{(i)})} V_{0,s}^{(i,l)}, \quad (10)$$

$$n_{Mi,l} = \sum_{k=1}^{K-1}\sum_{s=0}^{L-1} b_i^{(k)} \alpha_k^s\big(T_{sa}^{(i)}\big) e^{j\theta_k^s(T_{sa}^{(i)})} V_{k,s}^{(i,l)}, \quad (11)$$

and $$n_{Wi,l} = \int_{T_{sa}^{(i-1)}}^{T_{sa}^{(i)}} a_0(t - lT_c) n_w(t)\, dt, \quad (12)$$

respectively, where

$$V_{k,s}^{(i,l)} \triangleq \sum_{n=T_{sa}^{i-1}/T_c}^{T_{sa}^{(i)}/T_c - 1} a_0((n-l)T_c) b_k((n-s)T_c - \tau_k) \times a_k((n-s)T_c - \tau_k)$$

is the interference on the lth path of the ith bit of the reference user from the sth path of the kth user.

As the user number $K \to \infty$, $n_{Mi,l}$ is asymptotically Gaussian by the central-limit theorem. Since the self-interference term becomes negligible when compared to the multi-access interference, we approximate the final test statistic as

$$g_{i,l} = AMb_i^{(0)} \alpha_0^l\big(T_{sa}^{(i)}\big) e^{j\theta_0^l(T_{sa}^{(i)})} + N_{i,l}, \quad (13)$$

where $N_{i,l}$ is zero-mean complex Gaussian with $\frac{1}{2}E[|N|^2] = \frac{1}{2}E[|n_M|^2] + \frac{1}{2}E[|n_W|^2]$, independent of both i and l.

For perfect interleaving, $\{g_{i,l}, i = 0, 1, \ldots; l = 0, \ldots, L-1\}$ are not only independent for different values of l, but also independent for different values of i. With perfect channel estimation, we can condition on $\alpha_k^l(T_{sa}^{(i)}) e^{j\theta_k^l(T_{sa}^{(i)})}$ and use the same technique as in [6] to determine performance. The decoded data for the 0th user is determined by finding the path in the trellis which minimizes the metric given by

$$D_v = \mathrm{Re}\left[\sum_{i=0}^{\infty}\sum_{l=0}^{L-1} \hat{b}_{i,v}^{(0)} g_{i,l} \alpha_0^l\big(T_{sa}^{(i)}\big) e^{-j\theta_0^l(T_{sa}^{(i)})}\right], \quad (14)$$

where the subscript v refers to a particular path in the trellis, and $\hat{b}_{i,v}^{(0)}$ is the ith code symbol along path v. We see that the decision rule (14) can be implemented by a maximal-ratio combining RAKE receiver (i.e., $\hat{c}_{i,l}^k = \alpha_0^l(T_{sa}^{(i)}) e^{-j\theta_0^l(T_{sa}^{(i)})}$) followed by an unweighted trellis decoder.

3.3. *Bit Error Performance*

For convolutional codes, the union bound of the bit error rate (BER) is

$$P_b \leq \sum_{d=d_{\mathrm{free}}}^{\infty} \gamma_d P_d, \quad (15)$$

where $\{\gamma_d\}$ is the distance spectrum, d_{free} is the free distance of the code, and P_d is the pairwise error probability of two sequences with distance d (assume they differ in the first d bits). Using the metric of (14), we have

$$\begin{aligned} P_d &= \mathrm{Prob}\left(\mathrm{Re}\left[\sum_{i=0}^{d-1}\sum_{l=0}^{L-1}\big(b_i^{(0)} - \hat{b}_{i,u}\big) g_{i,l}\alpha_0^l\big(T_{sa}^{(i)}\big) \times e^{-j\theta_0^l(T_{sa}^{(i)})}\right] < 0\right) \\ &= \mathrm{Prob}\left(\mathrm{Re}\left[\sum_{i=0}^{d-1}\sum_{l=0}^{L-1} 2b_i^{(0)} g_{i,l}\alpha_0^l\big(T_{sa}^{(i)}\big) \times e^{-j\theta_0^l(T_{sa}^{(i)})}\right] < 0\right). \end{aligned} \quad (16)$$

To get P_d, let $X_{i\times L+l} \triangleq \alpha_0^l(T_{sa}^{(i)})e^{j\theta_0^l(T_{sa}^{(i)})}$, and $Y_{i\times L+l} \triangleq b_i^{(0)} g_{i,l}$; then (16) can be written as

$$P_{\rm d} = \text{Prob}(\text{Re}\{X^*Y\} < 0). \tag{17}$$

Note that with uncorrelated channel fading, the above is a special case of [10, p. 882] where X_i and Y_i are a pair of correlated complex-valued Gaussian random variables. The dL pairs $\{X_i, Y_i\}$ are statistically independent and identically distributed. From (9), (11), and (12), we can obtain the second (central) moments as

$$\begin{aligned}
\mu_{xx} &= \frac{1}{2}E[X^*X] = \sigma^2 \\
\mu_{xy} &= \frac{1}{2}E[X^*Y] = AM\sigma^2 \\
\text{and} \quad \mu_{yy} &= \frac{1}{2}E[Y^*Y] \\
&= A^2M^2\sigma^2 + (K-1)LM\sigma^2 + \frac{N_0}{2}M.
\end{aligned}$$

From [11] and [10],

$$\begin{aligned}
P_{\rm d} &= \frac{-1}{2\pi j}\int_{-\infty+j\varepsilon}^{+\infty+j\varepsilon} \frac{(v_1v_2)^{dL}}{v(v+jv_1)^{dL}(v-jv_2)^{dL}}\,dv \\
&= \frac{1}{(1+v_2/v_1)^{2dL-1}}\sum_{i=0}^{dL-1}\binom{2dL-1}{i}\left(\frac{v_2}{v_1}\right)^i,
\end{aligned} \tag{18}$$

where

$$\begin{aligned}
v_1 &= \sqrt{w^2 + \frac{4}{\mu_{xx}\mu_{yy} - |\mu_{xy}|^2}} - w, \\
v_2 &= \sqrt{w^2 + \frac{4}{\mu_{xx}\mu_{yy} - |\mu_{xy}|^2}} + w, \\
\text{and} \quad w &= \frac{2\text{Re}\mu_{xy}}{\mu_{xx}\mu_{yy} - |\mu_{xy}|^2}.
\end{aligned}$$

Substituting (18) into (15), we take $\gamma_{d_{\rm free}} P_{d_{\rm free}}$ and $\sum_{d=d_{\rm free}}^{+\infty} \gamma_d P_d$ to lower bound and upper bound the decoded BER, respectively. The uncoded BER can also be evaluated using P_1. Figure 4 shows the bit error rates

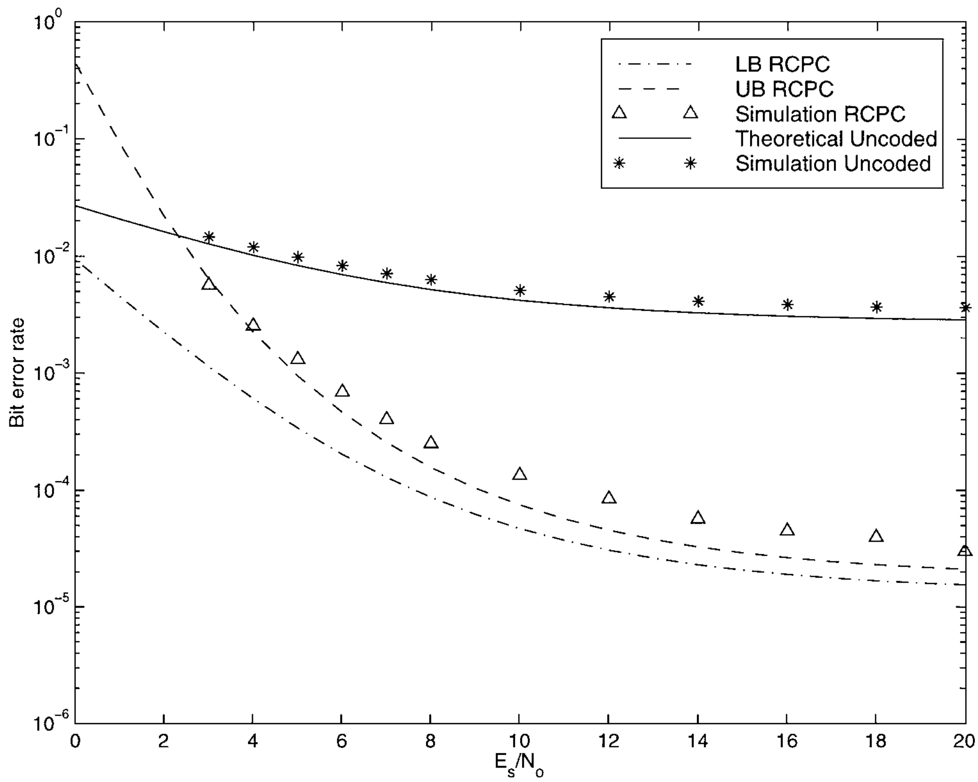

Figure 4. Theoretical results and simulation results. 10 users, 4 multipaths, uncorrelated Rayleigh fading.

for an uncoded bit stream as well as for the coded bit stream using the convolutional code from [9, Table II, b, code rate 8/9], where E_s/N_0 is the ratio of energy-per-coded-bit to noise power spectral density. In the figure, it is seen that most of the simulation results are higher than the upper bound. This occurs because we have not considered self-interference in the analysis, and because we have truncated the infinite sum of (15) to 6 terms [9].

When the fading in the channel is correlated, the above analysis fails for the coded bit error rate, so we use simulation to get the desired results. The Jakes model [12, 13] is used to generate time-correlated Rayleigh fading parameters $c_i^k(t)$ for the L independent paths of each user.

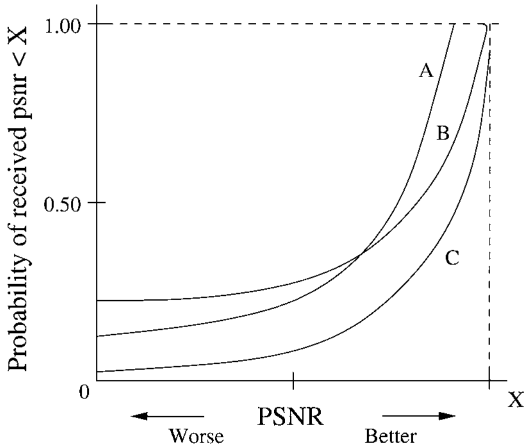

Figure 5. Comparison of CDF curves.

4. Results

Equation (1) defines a 3-dimensional surface on which every point (r_s, r_c, M) corresponds to a possible bandwidth allocation that the communication system could, in theory, use. We wish to find the point on the surface which has the best performance. We let $F(r_s, r_c, M)$ denote the performance of the system. The choice of a good set of system parameters depends on the performance measure and the channel conditions. For a given system, both the fades and the noise in the channel are random processes. Therefore, the output from the source decoder is not the same for different trials. We measure the performance of the system by looking at the output for many independent trials. The Peak Signal-to-Noise Ratio (PSNR) is defined as $10 \log \frac{\textit{peak image energy}}{\textit{mean square error } (MSE)}$, where $MSE = E[(\textit{received image} - \textit{original image})^2]$, and *peak image energy* $= 255^2$ for 8 bits per pixel grey scale images. The empirical cumulative distribution function (CDF) of the PSNR of the decoded images incorporates the randomness of the channel by showing the percentage of the received images which have a quality less than a certain value. For each possible set of system parameters, we can generate the CDF curve corresponding to that set. In this work, we assume that the performance of the system, F, is taken to be some summary statistic of the CDF curve, such as the area above the curve [14]. Our criterion for determining when the CDF curve has converged is as follows. We run an initial number J of random simulations of the channel, where J is at least 500, and we generate the CDF curve and compute our summary statistic from it. We run another J random simulations of the channel, and compute the CDF curve and its summary statistic from the $2J$ trials. If the new statistic is within 1% of the first one, we judge that the curve has converged, and use that result. In most cases, no further trials were required. If the difference exceeded 1%, we ran a last group of J random trials and combined the results again. In our experiments, the difference in the CDF metric and the previous one at this point was always less than 1%, and no further trials were required. For all plots, we ended up using between 1000 and 4000 random realizations of the channel.

Figure 5 illustrates what the CDF curves could look like. Each curve is the CDF of many trials, and shows the performance of a given system under one set of parameters. When two curves do not cross (e.g., curves A and C, or curves B and C), the lower curve is superior because it always has a higher probability of achieving PSNR values above any given PSNR. When there are crossovers between two curves (e.g., curves A and B), one may be superior for one application but not for another. Comparison of the curves may then involve maximizing the area above the curve, perhaps with some weighting (e.g., all PSNRs less than a certain amount may be considered equally bad, and all PSNRs above a certain amount may be considered equally good). The application requirements can sometimes be summarized by saying that a given image quality must be present at least a specified fraction of the time. For example, at most 5% of the time can the decoded images have PSNR below 20 dB. Some curves may then be inadmissible. These issues are discussed in [14].

Finding the optimal point can of course be done by exhaustive search. For each 3-tuple $(r_s,\ r_c,\ M)$ under consideration, we simulate a certain number of realizations of the lossy channel, and examine the decoded image quality for each realization to form the CDF curve. In any case where curves do not cross, we know the best performance corresponds to the lowest curve. When curves cross, we compute the final performance F as some summary statistic of this curve, and we find the best F.

We can separate the procedure of finding the optimal point into two steps:

Step 1. For every value of r_s, find the optimal pair $(r_c(r_s),\ M(r_s))$ under the constraint $\frac{1}{r_c} \cdot M = C_1/r_s = C_2$, where C_2 is a constant.
Step 2. Find the optimal point from the sets $\{r_s,\ r_c(r_s),\ M(r_s)\}$.

This is still an exhaustive search. However, for a fixed value of r_s (and with all other parameters of the system fixed except for r_c and M), the curves obtained by varying r_c and M (under the constraint $\frac{1}{r_c} \cdot M = C_2$) do not cross (see discussion below). So the lowest curve is the best, and one does not need to compute the summary statistic F for step 1. More substantial computational savings can be realized if the system satisfies the following property: For a fixed r_s (or $\frac{1}{r_c}M = C_2$), F is a monotonic function of some parameter, denoted by λ, such as BER, packet erasure rate, etc. Note that λ can often be obtained from r_c and M easily by either theoretical analysis or relatively simple simulations. An example is provided below. In this case, *Step 1* is significantly simplified.

4.1. Tradeoffs of r_c and M Under the Constraint $\frac{1}{r_c}M = C_2$

For all the comparisons, we keep the ratio of energy-per-source-bit to noise power spectral density, E_b/N_0, constant. Figure 6 is a typical example which shows the tradeoff between channel code rate and processing gain using the CDF curves. Here $C_1 \approx 22.8$, the number of users $K = 10$, $E_b/N_0 = 3$ dB, $L = 4$, and the fading is correlated with normalized Doppler $f_D T_c = 1.93 \times 10^{-5}$. The parameters on each curve are (r_c, M). We use a delay constrained interleaver size where the total delay is equal to roughly $1658880 T_c$. For example, for a processing gain of 72, we use an interleaver of size 20 by 16 coded bits; for a processing gain of 36, we use an interleaver of size 40 by 16 coded bits. For each plot, since the source code rate is fixed, the best achievable image quality is the same for all curves. The curves do not cross, and it is easy to see how the system performance changes as the parameters change, and thus to decide which curve represents the best set of parameters. For example, in Fig. 6(b), for the sequence of channel code rates $r_c = 0.80, 0.60, 0.46, 0.36, 0.30$, approximately 13%, 64%, 84%, 91%, 94%, respectively, of the decoded images have PSNR larger than 29 dB. In this scenario, the system improves when more bandwidth is allocated to the channel coding (r_c decreases). The lowest curve ($r_c = 0.30$, $M = 48$) is the best curve.

Note that for a fixed C_2, when the bandwidth allocated to channel coding increases ($r_c \downarrow$), the bandwidth allocated to spreading decreases ($M \downarrow$). Thus there are two counterbalancing effects. Assume we have a set of error correcting codes where a lower value of r_c corresponds to a larger coding gain; at the same time, M decreases and this causes both loss of some diversity enhancement and a decrease in interference suppression, both of which degrade the system performance. This degradation resulting from a small processing gain can be observed in Fig. 6(d). As the processing gain decreases from 36 to 30, even though we have a stronger error correction code, the performance of the system degraded.

From the simulation, we observed empirically that, given the channel and a fixed set of parameters, $E_b/N_0,\ f_D T_c,\ L$ and K, along with a fixed interleaver delay constraint, for a given r_s, a lower BER always corresponded to a lower curve and thus a better system. In other words, if we let $\lambda = BER$, then the system performance F is a monotonic function of λ. In this case, we can easily determine the best (r_c, M) pair for a fixed r_s. BER values of all the curves from Fig. 6 are listed in Table 1; they yield the same optimal sets of parameters as do the CDF curves. Note that to get an accurate CDF curve, we normally need 10 to 40 times more trials in the simulation than what is needed for an accurate BER estimate.

In the case of perfect interleaving, we can use the theoretical BER bounds derived in Section 3.3, and further reduce the amount of work by ignoring those (r_c, M) pairs whose lower bounds lie above the upper bounds of any other pair.

4.2. Tradeoffs of r_s and $\frac{1}{r_c}M$

After we find the optimal $(r_c(r_s),\ M(r_s))$ for each r_s, we plot the CDF curves for each 3-tuple. Figure 7 shows the best curves from Fig. 6. The parameters on each curve are (r_s, r_c, M). For the top curve, we see that there is a higher probability that the output image has a low

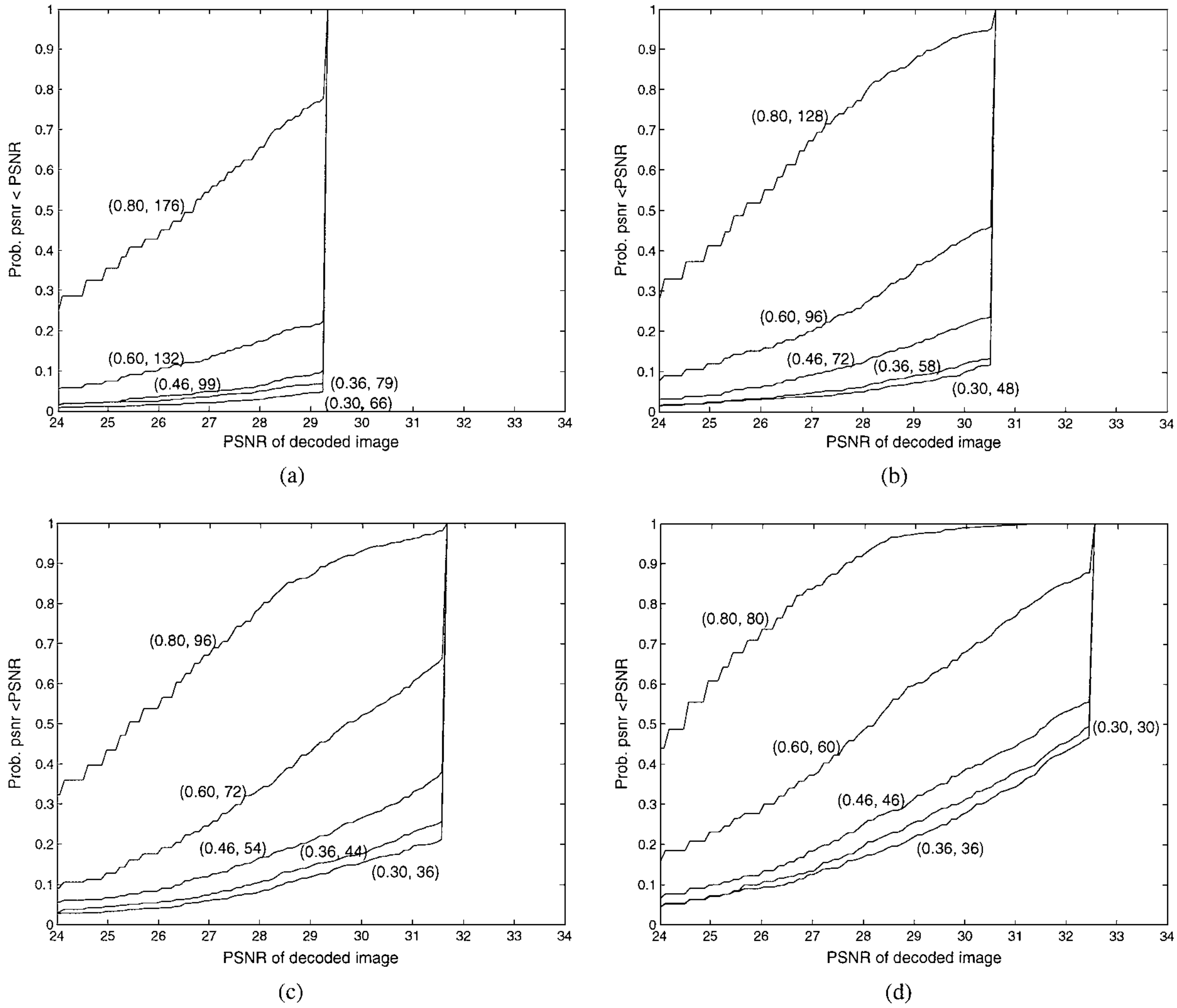

Figure 6. CDF plots: Tradeoff between channel code rate and processing gain. $K = 10$, $E_b/N_0 = 3$ dB and $L = 4$. Normalized Doppler $f_D T_c = 1.93 \times 10^{-5}$. (a) $r_s \approx 0.104$ bpp, $C_2 \approx 220$, (b) $r_s \approx 0.143$ bpp, $C_2 \approx 160$, (c) $r_s \approx 0.189$ bpp, $C_2 \approx 120$ and (d) $r_s \approx 0.228$ bpp, $C_2 \approx 100$.

PSNR (only 77% of the decoded images have PSNR above 29 dB). But since more bandwidth is allocated to source coding, the best achievable PSNR is larger than that of all the other curves (the right end of the curve reaches a PSNR of 32.59 dB). In contrast, for the lowest curve, there is a higher probability of achieving PSNR above 29 dB (96%). But with less bandwidth allocated to source coding, the best PSNR achievable is limited to 29.36 dB, lower than the corresponding values of the other curves.

Table 1. BER of curves in Fig. 6.

r_c	(a)	(b)	(c)	(d)
0.80	4.87×10^{-3}	8.31×10^{-3}	1.05×10^{-2}	1.70×10^{-2}
0.60	4.16×10^{-4}	8.44×10^{-4}	1.38×10^{-3}	2.57×10^{-3}
0.46	1.12×10^{-4}	2.61×10^{-4}	3.44×10^{-4}	5.20×10^{-4}
0.36	8.35×10^{-5}	1.28×10^{-4}	2.28×10^{-4}	3.97×10^{-4}
0.30	4.76×10^{-5}	9.56×10^{-5}	1.73×10^{-4}	4.28×10^{-4}

To give an idea of the resulting visual quality, Fig. 8 shows the decoded images at 29.36 dB and 32.59 dB. The image at 29.36 dB is significantly blurrier than the one at 32.59 dB. These images correspond to the maximum achievable quality of the system with $r_s = 0.104$ bpp and $r_s = 0.228$ bpp of Fig. 6, respectively.

In this case, where there are crossovers between the curves, the criterion to choose the best curve depends

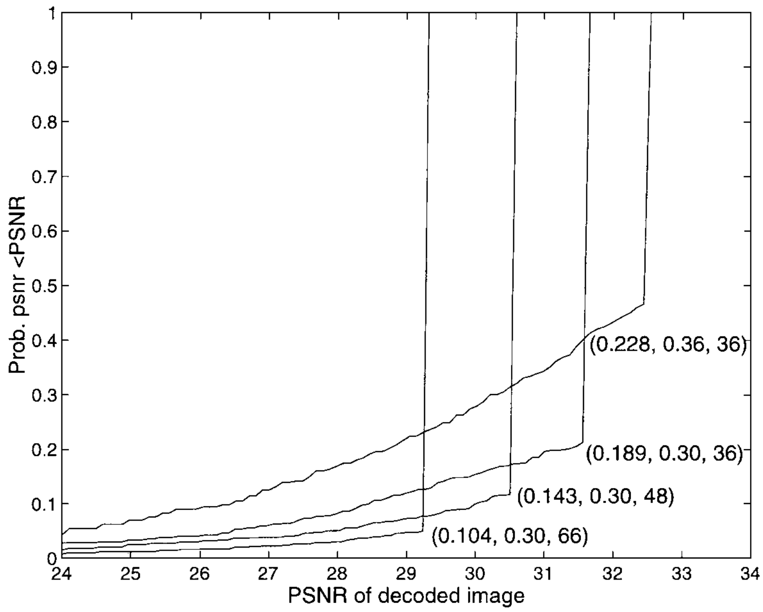

Figure 7. CDF plots: Tradeoff among source code rate, channel code rate and processing gain. User number $K = 10$, $E_b/N_0 = 3$ dB and $L = 4$. Normalized Doppler $f_D T_c = 1.93 \times 10^{-5}$.

(a) (b)

Figure 8. Decoded images. (a) $r_c = 0.104$ bpp, $PSNR = 29.36$ dB. (b) $r_c = 0.228$ bpp, $PSNR = 32.59$ dB.

on the application requirements. One way to evaluate the curve is to compute $F(r_s, r_c, M)$ as the unweighted area under the corresponding MSE CDF curves as in [14]. According to this criterion, (0.189, 0.30, 36) is considered optimal among the set of curves.

4.3. Tradeoffs Related to Channel Estimation

The results above all corresponded to perfect estimation of the channel gains and phases. To incorporate the effects of imperfect channel state estimation, we employ the block diagram of Fig. 9, which shows an estimation method appropriate for BPSK signals [10, p. 803]. The figure shows only the estimation technique on one tap. We use an integrate and dump for the low pass filter over the interval $(t - BT, t)$, where B is called the estimation length.

Figure 10 shows the BER performance versus estimation length B for a fixed r_s, r_c and M. We assume a carrier frequency of $f_c = 900$ MHz, and a

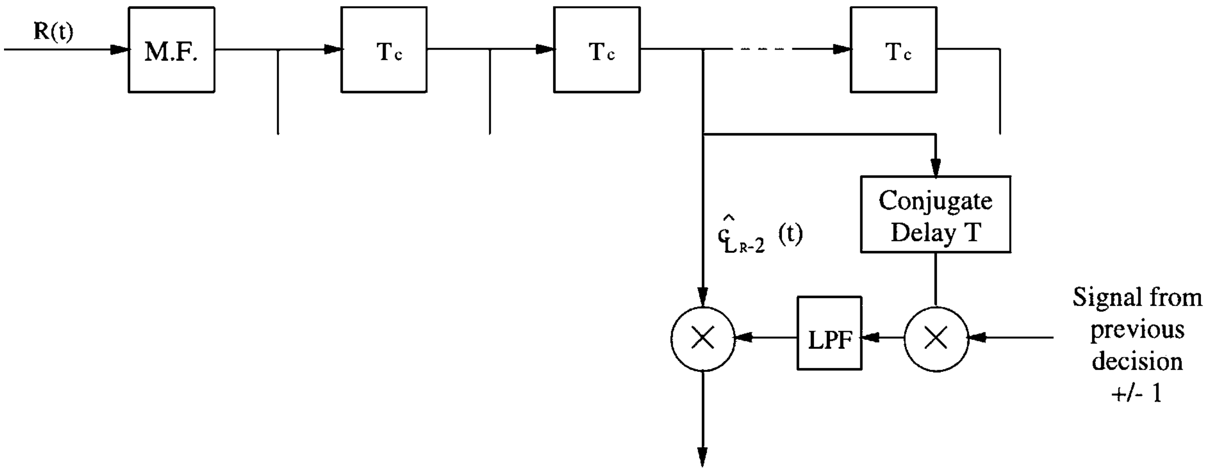

Figure 9. Channel tap weight estimation with BPSK signal.

data rate of 29 K bits/sec; the two plots correspond to mobile speeds of 30 mph and 70 mph, respectively, with parameters $r_c = 0.46$, $M = 72$, $K = 4$, and $L = 4$. Here we use the same delay constraint for the interleaver as in Section 4.1—interleaver size 20 by 16 coded channel bits for processing gain 72. From the figure, we see that $B \approx \frac{1}{15}\frac{1}{f_D T} = \frac{1}{15M} \cdot \frac{1}{f_D T_c}$, i.e., around 40 and 20, respectively, gives the best BER performance for these two cases. When B is too small, the estimate is degraded by the noise and interference; when B is too large, the channel changes too rapidly for the estimates to be useful.

Figure 11 shows the tradeoffs when channel estimation is employed. The optimal ($B = \frac{1}{15M} \cdot \frac{1}{f_D T_c}$) is used. $K = 4$, $E_b/N_0 = 4\,\text{dB}$, $L = 4$, $f_D T_c = 1.93 \times 10^{-5}$, and the parameters beside the curves are (r_c, M). The interleaver delay constraint is the same as in Section 4.1. Note that in this plot, as more bandwidth is allocated to channel coding (r_c decreases), the system first improves when r_c decreases from 0.80 to 0.60 to 0.46, and then deteriorates when additional bandwidth is allocated to the coding (r_c decreases to 0.36 then to 0.30).

We also observe that F is not a monotonic function of BER for a fixed r_s when channel estimation is employed (for example, in Fig. 11, BER's for the top curve to the bottom curve are 1.72×10^{-2}, 1.66×10^{-2}, 3.73×10^{-2}, 4.04×10^{-2} and 2.74×10^{-2} respectively). Therefore, we cannot exploit the computational savings referred to above in determining the best triple (r_s, r_c, M).

4.4. Effects of Interleaving

The source decoding algorithm, the channel decoding algorithm and the deinterleaver might cause significant delays in the system, especially for time critical applications such as voice and video transmissions. Here we discuss the effects of the interleaver.

Generally, a larger deinterleaver will scatter correlated errors further apart. However, this does not always benefit the system, especially when the system performance depends more on packet erasure rate than on bit error rate (recall that the decoded image is reconstructed from the bit stream up to the first lost packet). Figure 12 shows the system performance versus interleaver size under different channel conditions. The channel coding rate is 0.80. There are $K = 6$ active users, the processing gain is 128, and E_b/N_0 is 4 dB. We see that a larger interleaver size does not necessarily lead to better performance. With dispersed errors, more packets are affected. Even though that dispersion of errors results in fewer errors per packet, the number of those bit errors may still be large enough to overwhelm the decoder. In such a case, the dispersion of errors causes a larger number of packets to experience decoding failure. When the deinterleaver size gets sufficiently large, the errors are, in turn, sufficiently dispersed so that they can get corrected and the final quality improves. For the curves shown in Fig. 12, the deinterleaver size has to be about 120 by 120 coded bits before the decoder functions efficiently.

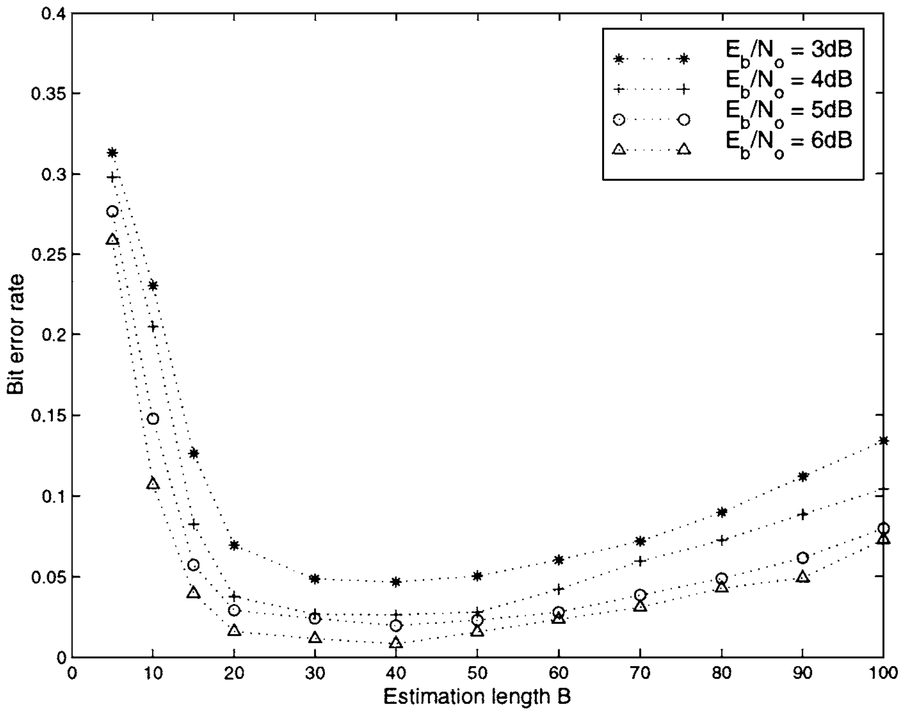

(a)

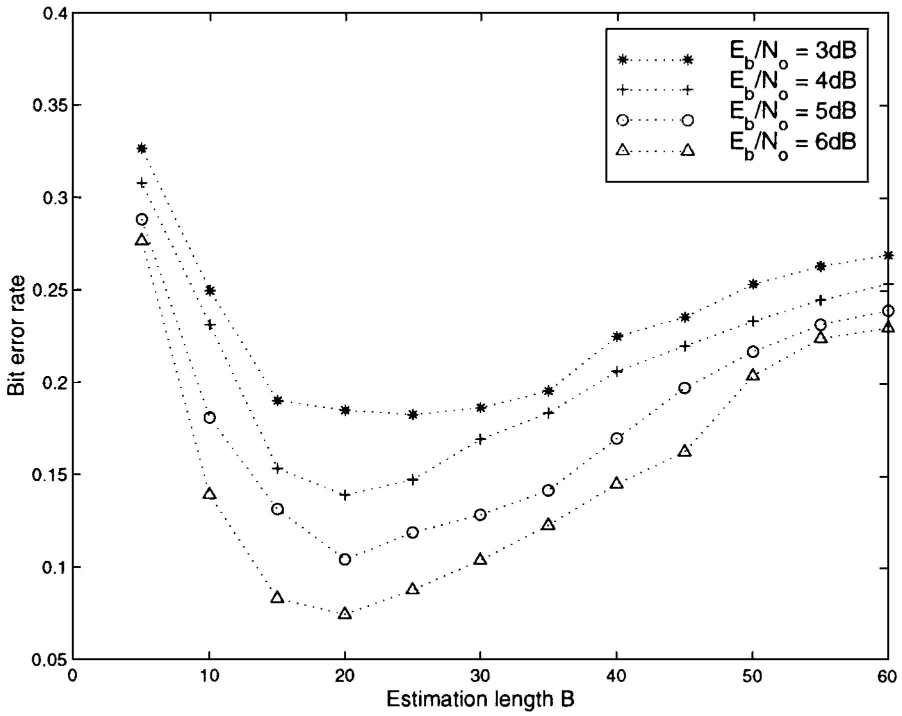

(b)

Figure 10. Bit error rate versus channel estimation length. Processing gain $M = 72$, number of users $K = 4$, and multi-path $L = 4$. Interleaver 20 by 16 coded bits. (a) $f_D T_c = 1.93 \times 10^{-5}$. (b) $f_D T_c = 4.50 \times 10^{-5}$.

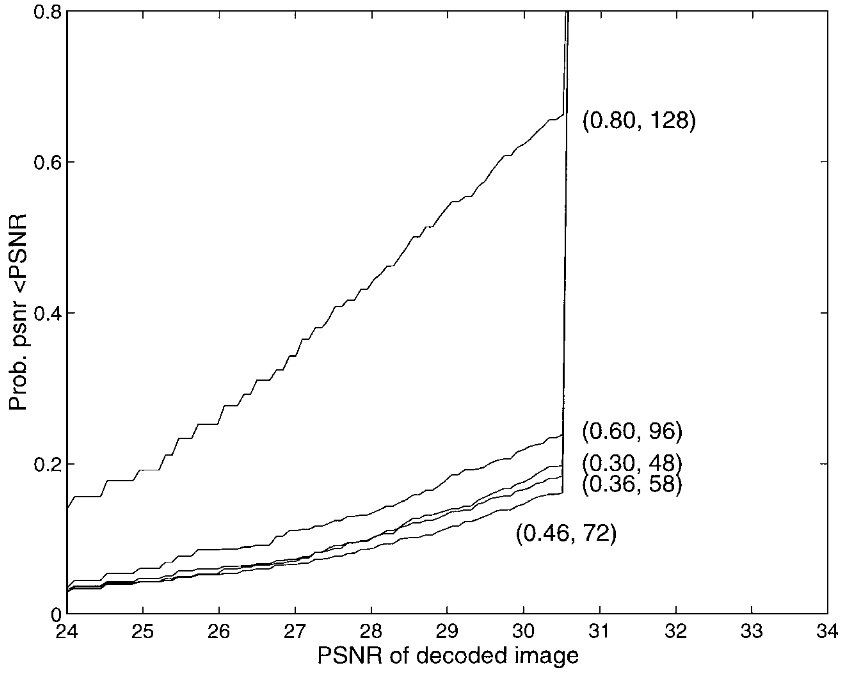

Figure 11. CDF plots: Tradeoff between r_c and M with channel estimation. $K = 4$, $E_b/N_0 = 4$ dB, $L = 4$, $r_s \approx 0.143$ bpp, $C_2 \approx 160$. Normalized Doppler $f_D T_c = 1.93 \times 10^{-5}$.

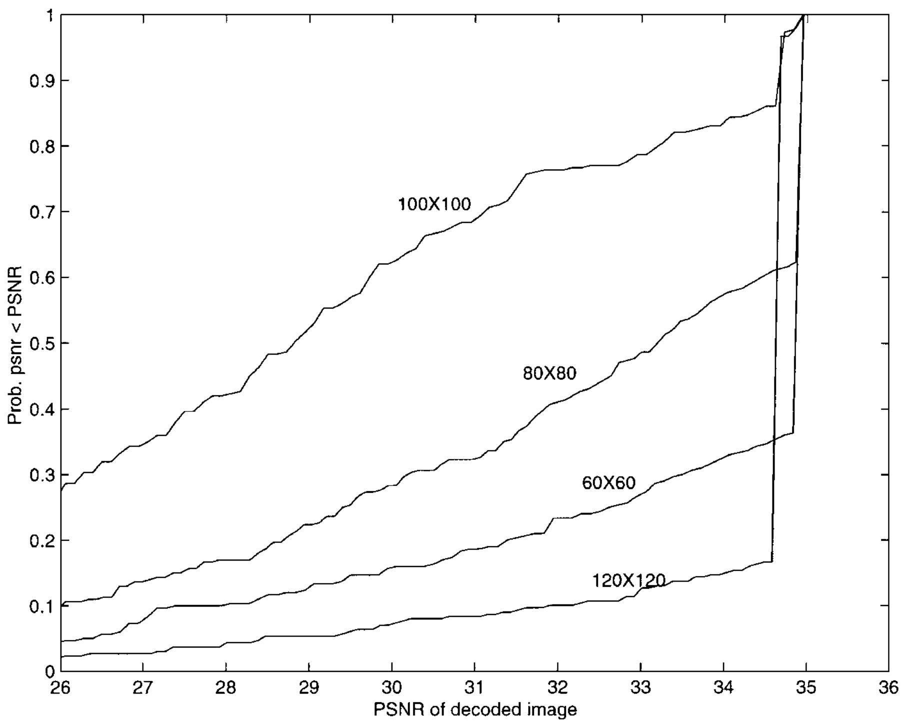

Figure 12. System performance parameterized by interleaver size. $K = 6$, $E_b/N_0 = 4$ dB, $L = 4$, $M = 128$. $r_c = 0.80$, and packet size 250. Normalized Doppler $f_D T_c = 1.46 \times 10^{-6}$.

5. Conclusions

In this paper, we introduce three-way tradeoffs among source coding, channel coding and spreading in CDMA systems. For a fixed bandwidth, the performance of the system is quantified by the CDF curves of the decoded images. A two step method is employed to obtain the optimal bandwidth allocation represented by the CDF curves. Under certain constraints, the two step optimization method significantly reduces the amount of computation.

We show that allocating more bandwidth to source coding allows us to achieve a higher maximum image quality, but the probability of achieving this quality is smaller. On the other hand, allocating more bandwidth to channel coding and spreading decreases the number of source information bits transmitted and thus limits the best achievable image quality, but the probability of achieving this quality is higher. For a fixed source coding rate, allocating more bandwidth to channel coding gives us a stronger code; but since less bandwidth is left for processing gain, there is a loss of diversity enhancement and a decrease in interference suppression; in the case of imperfect channel estimation, a smaller processing gain can also lead to a poorer estimate and thus a degradation in the system performance.

Acknowledgments

This research was partially sponsored by the Center for Wireless Communications of UCSD, and by the CoRe program of the State of California.

References

1. B.D. Pettijohn, K. Sayood, and M.W. Hoffman, "Joint Source/Channel Coding Using Arithmetic Codes," *IEEE Proceedings DCC 2000. Data Compression Conference*, March 2000, pp. 73–82.
2. G. Cheung and A. Zakhor, "Bit Allocation for Joint Source/Channel Coding of Scalable Video," *IEEE Transactions on Image Processing*, vol. 9, no. 3, 2000, pp. 340–356.
3. M. Zhao, A.A. Alatan, and A.N. Akansu, "A New Method for Optimal Rate Allocation for Progressive Image Transmission Over Noisy Channels," *Proceedings DCC 2000. IEEE Data Compression Conference*, March 2000, pp. 213–222.
4. D.J. Van Wyk, I.J. Oppermann, and L.P. Linde, "Performance Tradeoff Among Spreading, Coding and Multiple-Antenna Transmit Diversity for High Capacity Space-Time Coded DS/CDMA," *Proceedings of Conference on Military Communications MILCOM 1999*, Sept. 1999, vol. 1, pp. 393–397.
5. I. Oppermann and B. Vucetic, "Capacity of a Coded Direct Sequence Spread Spectrum System Over Fading Satellite Channel Using an Adaptive LMS-MMSE Receiver," *IEICE Trans. Fundamentals*, vol. E79-A, no. 12v, 1996, pp. 2043–2049.
6. J.R. Foerster and L.B. Milstein, "Coding for a Coherent DS-CDMA System Employing an MMSE Receiver in a Rayleigh Fading Channel," *IEEE Transactions on Communication*, vol. 48, no. 6, 2000, pp. 1012–1021.
7. A. Said and W.A. Pearlman, "A New, Fast, and Efficient Image Codec Based on Set Partitioning in Hierarchical Trees," *IEEE Transactions on Circuits and Systems for Video Technology*, vol. 6, no. 3, 1996, pp. 243–250.
8. P.G. Sherwood and K. Zeger, "Progressive Image Coding on Noisy Channels," *IEEE Signal Processing Letters*, vol. 4, no. 7, July 1997, pp. 189–191.
9. J. Hagenauer, "Rate-Compatible Punctured Convolutional Codes (RCPC Codes) and Their Applications," *IEEE Transactions on Communication*, vol. 36, April 1988, pp. 389–400.
10. J.G. Proakis, *Digital Communications*, New York: McGraw-Hill, 1995.
11. L.L. Chong, "The Effects of Channel Estimation Error on Wideband CDMA Systems with Path, Frequency, Time, and Space Diversity," Ph.D. Dissertation, University of California, San Diego, 2001.
12. W.C. Jakes, *Microwave Mobile Communications*, Piscataway, NJ: IEEE Press, 1993c 1974.
13. P. Dent, G.E. Bottomley, and T. Croft, "Jakes' Model Revisited," *Electronics Letters*, vol. 29, no. 13, 1993, pp. 1162–1163.
14. P.C. Cosman, J.K. Rogers, P.G. Sherwood, and K. Zeger, "Combined Forward Error Control and Packetized Zerotree Wavelet Encoding For Transmission of Images Over Varying Channels," *IEEE Transactions on Image Processing*, June 2000, pp. 982–993.

Qinghua Zhao was born in Shannxi, China, in 1976. She received the B.S. degree in electrical engineering, at Xi'an JiaoTong University, Xi'an, China, in 1996, and the M.S. in electrical engineering, at the University of California, San Diego (UCSD), in 2000. She is currently a Graduate Student Researcher at the University of California, San Diego, working toward the Ph.D. degree. Her research interests are in the area of communication theory, information theory, channel coding and spread-spectrum. She is a student member of IEEE.
qizhao@ucsd.edu

Pamela Cosman obtained her B.S. with Honor in Electrical Engineering from the California Institute of Technology in 1987, and her M.S. and Ph.D. in Electrical Engineering from Stanford University in 1989 and 1993, respectively. She was an NSF postdoctoral fellow at Stanford University and a Visiting Professor at the University of Minnesota during 1993–1995. Since July of 1995, she is on the faculty of the department of Electrical and Computer Engineering at the University of California, San Diego, where she is currently an associate professor. Her research interests are in the areas of data compression and image processing. Dr. Cosman is the recipient of the ECE Departmental Graduate Teaching Award (1996), a Career Award from the National Science Foundation (1996–1999), and a Powell Faculty Fellowship (1997–1998). She is an associate editor of the IEEE Communications Letters, and was a guest editor of the June 2000 special issue of the IEEE Journal on Selected Areas in Communications on "Error-resilient image and video coding." She was the Technical Program Chair of the 1998 Information Theory Workshop in San Diego, and is a Senior Member of the IEEE, and a member of Tau Beta Pi and Sigma Xi. Her web page address is http://www.code.ucsd.edu/cosman/
pcosman@ucsd.edu

Laurence B. Milstein received the B.E.E. degree from the City College of New York, New York, in 1964, and the M.S. and Ph.D. degrees in electrical engineering from the Polytechnic Institute of Brooklyn, Brooklyn, NY, in 1966 and 1968, respectively.

From 1968 to 1974, he was with the Space and Communication Group of Hughes Aircraft Company, and from 1974 to 1976, he was a Member of the Department of Electrical and Systems Engineering, Rensselaer Polytechnic Institute, Troy, NY. Since 1976, he has been with the Department of Electrical and Computer Engineering, University of California at San Diego (UCSD), La Jolla, where he is a Professor and former Department Chairman, working in the area of digital communication theory with special emphasis on spread-spectrum communication systems. He has also been a consultant to both government and industry in the areas of radar and communications.

Dr. Milstein was an Associate Editor for communications Theory for the IEEE TRANSACTIONS ON COMMUNICATIONS, an Associate Editor for Book Reviews for the IEEE TRANSACTIONS ON INFORMATION THEORY, an Associate Technical Editor for the IEEE COMMUNICATIONS MAGAZINE, and Editor-in-Chief of the IEEE JOURNAL ON SELECTED AREA IN COMMUNICATIONS. He was the vice President for Technical Affairs in 1990 and 1991 of the IEEE Communications Society and has been a member of the Board of Governors of both the IEEE Communications Society and the IEEE Information Theory Society. He has been a member of the IEEE Fellows Selection Committee since 1996, and he currently is the Chair of that committee. He is also the Chair of ComSoc's Strategic Planning Committee. He is a recipient of the 1998 Military Communications Conference Long-Term Technical Achievement Award, an Academic Senate 1999 UCSD Distinguished Teaching Award, an IEEE Third Millenium Medal, and the 2000 IEEE Communication Society Armstrong Technical Achievement Award.
lmilstein@ucsd.edu